

Polymeric Flower-Like Microparticles from Self-Assembled Cellulose Stearoyl Esters

Kai Zhang,^{*,†} Andreas Geissler,[†] Xuelian Chen,[‡] Sabine Rosenfeldt,[‡] Yongbiao Yang,[§] Stephan Förster,[‡] and Florian Müller-Plathe[§]

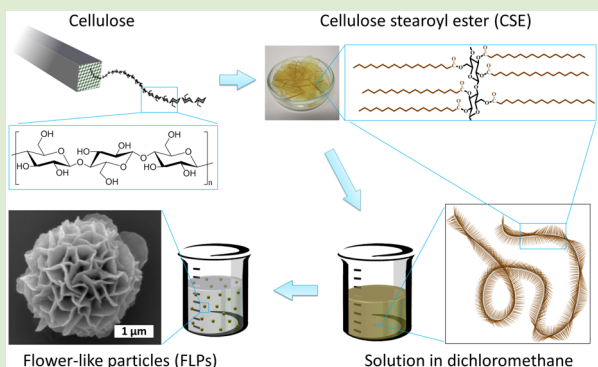
[†]Ernst-Berl-Institute for Chemical Engineering and Macromolecular Science, Technische Universität Darmstadt, Alarich-Weiss-Str. 8, 64287 Darmstadt, Germany

[‡]Physical Chemistry I, University of Bayreuth, Universitätsstrasse 30, 95440 Bayreuth, Germany

[§]Eduard-Zintl-Institute for Inorganic and Physical Chemistry, Technische Universität Darmstadt, Alarich-Weiss-Str. 4, 64287 Darmstadt, Germany

S Supporting Information

ABSTRACT: Flower-like particles (FLPs) with hierarchical surface architectures have recently attracted considerable attention due to their potentially wide application range. Hitherto, nearly all FLPs were fabricated using inorganic compounds, while versatile organic polymers have not received sufficient attention yet. Herein, we show the construction of novel organic, polymeric FLPs with diameters of 2.5–5 μm using cellulose stearoyl esters (CSEs) by means of the crystallization of side chains. CSEs with degrees of substitution of approximately 3 were transformed into FLPs during the gradual precipitation of polymer chains from the mixture of their solutions in dichloromethane (DCM) and a nonsolvent, which is driven by the evaporation of DCM. Ordered petal-like nanostructures were formed on the particle surface through the crystallization of side chains. Finally, partially crystalline FLPs containing lamellar structures were obtained. Moreover, the formation process was strongly affected by the molecular weight of CSE, concentrations of CSE solutions and the volume ratio between DCM and nonsolvents.



Nano- and microparticles with controllable hierarchical architectures are of increasing interest, not only for the development of precisely controlled nanotechnology,^{1–4} but also for their broad application field ranging from catalysis,^{5,6} drug delivery,⁷ and energy harvesting,⁸ to electrode materials for batteries.^{2,3,9,10} Flower-like particles (FLPs), as one such nanosystem resembling the morphology of flowers, such as rose and dahlia, exhibit highly enhanced surface areas in comparison to closed spherical particles or core–shell particles.^{2,11–13} Hitherto, nearly all FLPs are based on inorganic compounds, such as carbon materials and various metal oxides.^{2,14,15} Inorganic FLPs have been used as substrates for organic compounds, for example, FLPs from calcium or copper phosphate as scaffolds for proteins including α -lactalbumin, laccase, lipase, and α -amylase,^{11,16,17} FLPs from zeolite for polymers including polystyrene and polydivinylbenzene (PDVB),¹⁸ as well as FLPs from fullerene C₆₀ for porphyrin-polymers.^{14,15} A major reason for using inorganic compounds is that they can form organized nanostructures on the particle surface via a controlled crystallization process.¹¹ Controlling the morphologies of micro- or nanoparticles from polymers is more challenging. Their direct synthesis from monomers by emulsion polymerization, or the transformation of polymers using microfluidics predominantly leads to spheres with smooth

surfaces.^{19,20} In comparison to inorganic compounds, the crystallization of polymers from a solution leads to either nonregular aggregates or to special particles, such as Janus or patchy particles from block copolymers. However, the particles generally show smooth or patchy surface.^{21,22} Only very few organic or polymeric compounds, such as polyaniline²³ and pyrimido[4,5-*d*]pyrimidine nucleoside,²⁴ are reported to be able to construct FLPs. However, the formation of FLPs using polyaniline was hitherto only realized during the oxidation polymerization using ammonium peroxydisulfate as oxidant. More pronounced FLPs were obtained, if higher content of ammonium peroxydisulfate was used for the polymerization. Pyrimido[4,5-*d*]pyrimidine nucleoside formed large FLPs with average diameter of 40 μm based on the formation of H-bonds. In the present work, we used a cellulose-based polymer, cellulose stearoyl ester (CSE; Figure 1a), for the construction of purely organic and polymeric FLPs with an average diameter of 2.5–5 μm through the crystallization of alkyl side chains during their precipitation.

Received: December 10, 2014

Accepted: January 22, 2015

Published: January 26, 2015

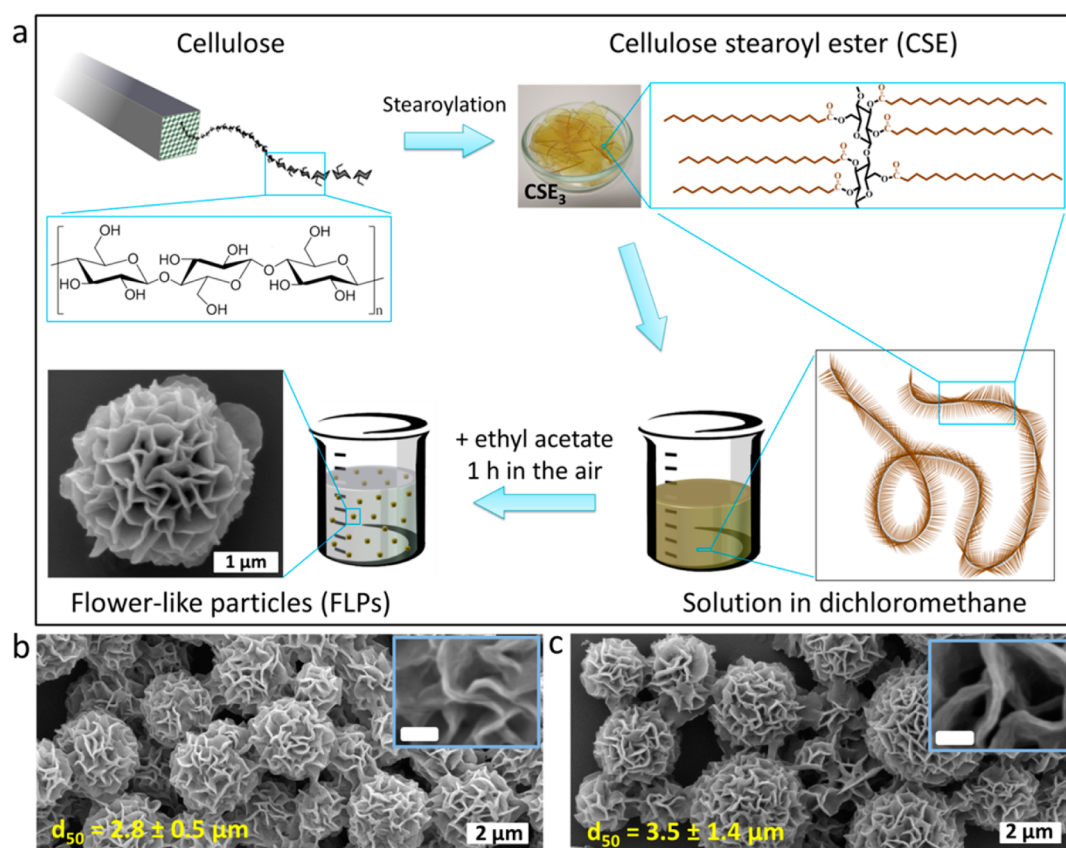


Figure 1. Fabrication of flower-like particles (FLPs). (a) Schematic representation for the synthesis of CSEs (details in Table S1) and the fabrication of FLPs. The photo image is representative for dried CSE₃. The scanning electron microscope (SEM) image shows a FLP from CSE₃, (b, c) SEM images of FLPs from (b) CSE_{2.97} and (c) CSE₃ with scale bars of 2 μm. The FLPs were obtained by adding 1 volume CSE solutions with the concentration of 10 mg/mL in dichloromethane into 3 volumes ethyl acetate and 1 h aging in air. The average diameters are calculated based on diameters of 50 individual particles (d_{50}). The insets show enlarged surface areas of FLPs with scale bars of 200 nm.

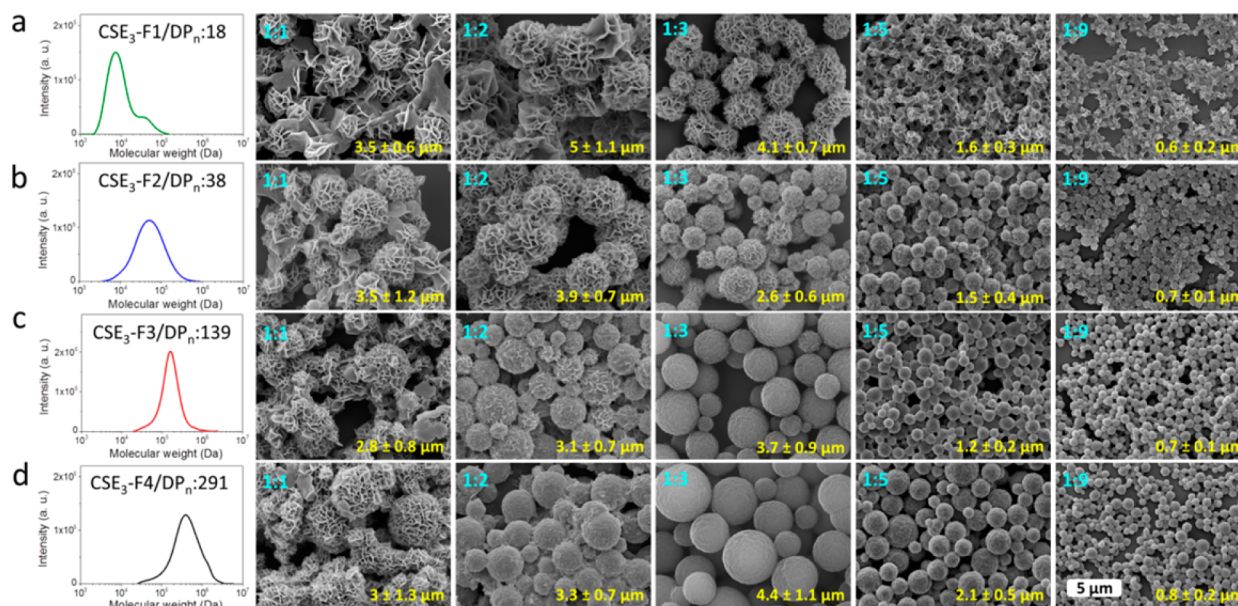


Figure 2. SEM images of particles from CSE₃ with different number-averaged degrees of polymerization (DP_n) of (a) CSE₃-F1, (b) CSE₃-F2, (c) CSE₃-F3, and (d) CSE₃-F4. Scale bar: 5 μm. The molecular weight distribution curves of CSE₃ fractions were obtained using size exclusion chromatography, leading to the determination of their DP_n . The particles were obtained after adding CSE₃ solution (10 mg/mL in DCM) into ethyl acetate at various volume ratios of 1:1, 1:2, 1:3, 1:5, and 1:9, as shown in cyan. The average diameters are d_{50} values.

Cellulose, a naturally occurring biopolymer, consists of β -(1 \rightarrow 4)-linked anhydroglucose units (AGUs) with three

hydroxyl groups per AGU that can be functionalized.²⁵ After the esterification using stearoyl chloride of 6 mol per mol

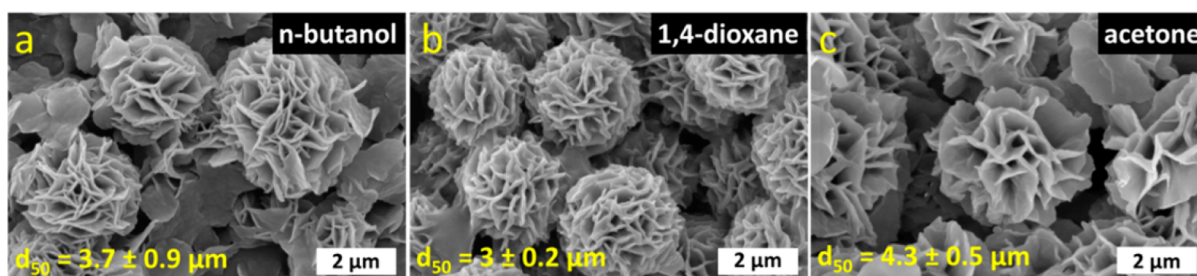


Figure 3. SEM images of FLPs obtained with other nonsolvents: (a) *n*-butanol, (b) 1,4-dioxane, and (c) acetone as precipitating medium. Scale bars: 2 μm . The volume ratio between DCM and each precipitant was 1:0.25. The average diameters are d_{50} values.

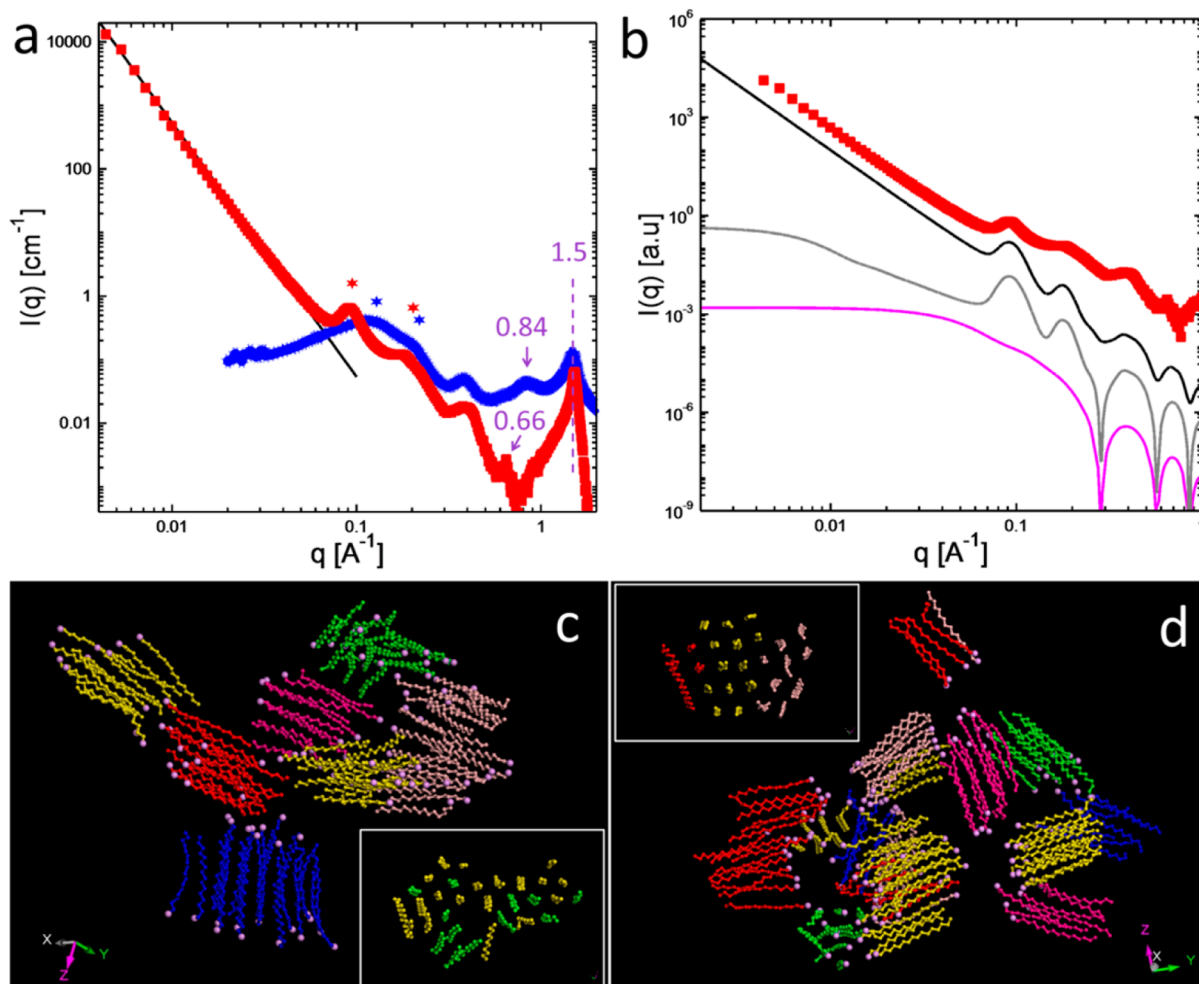


Figure 4. Analysis of the crystalline structure within FLPs. (a) 1D SAXS intensities of FLPs from CSE₃-F1 (red) and bulk CSE₃-F1 polymer (blue). 2D SAXS images are shown in Figure S13. The black line denotes a q^{-4} power law, arising from the mesoscopic dimensions of FLPs ($4.1 \pm 0.7 \mu\text{m}$). The stars represent the positions of Bragg reflections expected for a lamellar spacing. (b) 1D SAXS intensities of the FLPs (red) and the theoretical intensities based on the model of planar sheets with the diameter of 100 \AA and the thickness of 22 \AA . The magenta line denotes the model calculation assuming no interacting sheets. The model of five stacked planar sheets with a separation distance of 66 \AA is represented by gray line. Additional contributions by large scaled objects, following Porod's law (q^{-4}), are taken into account for the last model (black line). (c, d) Molecular structures formed after 100 ns of molecular dynamics simulations starting from two different initial solution states with (c) eight stretched single CSE₃ chains in regular arrangement and (d) one melt globule containing eight CSE₃ chains (Figures S14 and S15). The CSE₃ chains are present in EA molecules at the concentration of 4.8 wt %. Only the stearyl groups are shown for the visualization of crystalline regions. The larger atoms in pink represent the first C atoms after the carbonyl groups. The clusters are shown in distinct colors and the solvent molecules are not shown for clarity. The view along the stearyl axes of representative crystallites (insets) shows an approximately hexagonal packing of the alkyl chains from different CSE₃ chains within one crystallite. Within the same cluster as shown in the insets, the stearyl side chains from different CSE₃ are shown in distinct colors.

AGUs at 100 $^{\circ}\text{C}$ for 0.5 to 6 h, cellulose stearyl esters (CSEs) with degrees of substitution (DSs) between 2.8 and 3 were obtained (Figure 1a, Scheme S1). Only CSE with a DS of

≥ 2.97 , that is, with approximately complete derivatization of all hydroxyl groups by stearyl moieties, showed the capability to form FLPs (Figures 1b,c and S4a). In comparison, CSEs with

lower DSs of 2.92 or 2.88 only formed microparticles with rough, nonspecific surfaces. The FLPs exhibit highly porous and well-organized nanopetal-like surface architecture on their surface. The nanopetals have thicknesses between 30 and 80 nm (Figure 1b,c).

The concentration of polymer solutions in dichloromethane (DCM) is critical for the formation of FLPs. CSE solutions of 1 and 5 mg/mL in DCM only resulted in nano- and microparticles with rough surfaces (Figure S4b,c). FLPs with well-organized nanopetals were only observed by using solutions of higher concentrations, such as 10 mg/mL in DCM. The particle size increases with increasing concentrations of CSE solutions. Furthermore, FLPs from CSE with a DS of 2.97 (CSE_{2.97}) showed more uniform sizes with an average diameter of $2.8 \pm 0.5 \mu\text{m}$, compared to FLPs from CSE with a DS of 3 (CSE₃) with an average diameter of $3.5 \pm 1.4 \mu\text{m}$ (Figure 1b,c). A big difference between them is that CSE_{2.97} has a much lower number-averaged degree of polymerization (DP_n) of 36 than CSE₃ with a DP_n of 212 (Table S1). Hence, CSEs with lower DP_n are able to form more uniform FLPs under more lenient conditions.

In contrast to CSE_{2.97}, CSE₃ has a consistent chemical structure, because all hydroxyl groups at cellulose backbone are derivatized. Thus, CSE₃ was further used to study the formation process of FLPs. The effect of the molecular weight on the formation of FLPs was analyzed at first. For this purpose, a sample of CSE₃ was fractionated into four fractions (CSE₃-F1 to CSE₃-F4) by precipitation (Figure 2). These fractions exhibit different DP_n between 18 and 291 (Figure 2, Table S2). Starting from these CSE₃ fractions, FLPs of 2.5–5 μm or spherical micro/nanoparticles between 0.6 and 5 μm were obtained after the precipitation in ethyl acetate (EA) using the volume ratios of DCM/EA between 1:1 and 1:9 (Figure 2). The size and morphology of these particles highly depended on the molecular weight and the volume ratio of DCM/EA. CSE₃-F1 with a DP_n of 18 constituted FLPs at the DCM:EA ratio between 1:5 and 1:1, while CSE₃-F4 with a DP_n of 291 formed FLPs only at the DCM/EA of 1:1. Micro- or nanoparticles with smooth surfaces were generated from CSE₃-F4, if higher amounts of EA were used, for example, at the DCM/EA of 1:3, 1:5, or 1:9. CSE₃-F2 and CSE₃-F3 with the DP_n between those of CSE₃-F1 and CSE₃-F4 showed intermediate behaviors for the formation of FLPs. CSE₃-F2 with a DP_n of 38 began to form FLPs at the DCM:EA of 1:3, while CSE₃-F3 with a DP_n of 139 partially formed FLPs at the DCM/EA of 1:2 (Figure 2). In comparison to CSE₃ with higher DP_n , CSE₃ with lower DP_n could form FLPs using a broader ratio range of DCM/EA.

According to their solubility parameters, DCM is a good solvent for CSE₃, while EA is a poor solvent (Tables S5–S7, Figure S3). The formation of FLPs is therefore a slow precipitation process. However, more nanoscaled flakes were formed in addition to individual FLPs, if too much DCM was used, for example, at the DCM:EA of 1:1 (Figure 2a). The FLPs were also obtained using other solvents as precipitant, for example, *n*-butanol, 1,4-dioxane, and acetone (Figures 3 and S5). Due to the strong precipitating capability of these three solvents, only low amounts were required for the formation of FLPs, for example, using a volume ratio of DCM/precipitant of 1:0.25. Thus, the molecular weight of the polymer as well as the volume ratio between solvent (DCM) and precipitant are critical for the formation of FLPs.

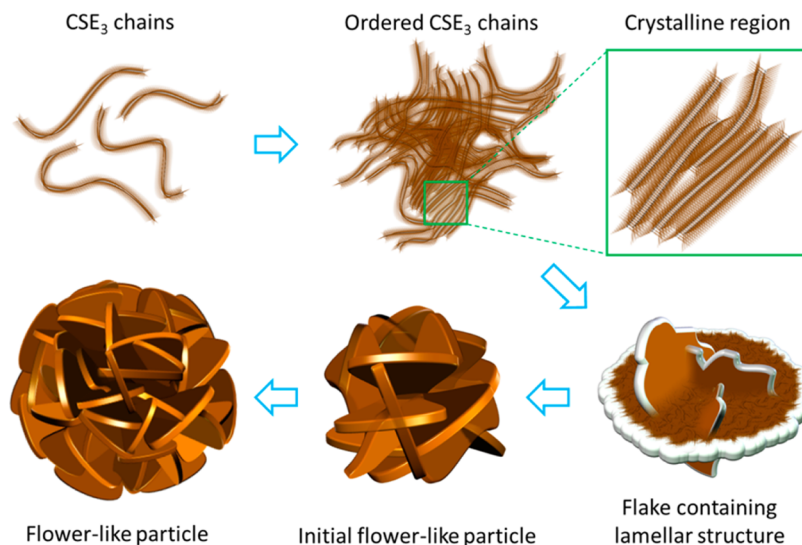
Due to potentially wide applications of FLPs, such as in (bio)catalysis, as drug-delivery systems and for gas sorption/

desorption, it is of great interest to elucidate the fundamental principle governing the formation of FLPs. The process during the formation of FLPs was studied by analyzing intermediates during the aging with SEM. Immediately after adding the CSE₃ solution into EA, CSE₃ was still dissolved in the mixture, as shown by DLS measurements (Figures S9–S11). The FLPs from CSE₃ were formed only after a certain aging time, for example, 60 min under ambient conditions (Figures S6 and S7). If DCM evaporated too fast from the mixture or the precipitation of CSE₃ was too fast, only flat flakes or nanoparticles were obtained (Figures S7 and S8).

Due to the difficulty for the in situ analysis of the particle formation, the crystalline structure within FLPs was further analyzed, in order to address the crystallization process for the particle formation. Differential scanning calorimetry (DSC) measurements suggested the presence of crystalline domains (Figure S12). To get a deeper insight, small-angle X-ray scattering (SAXS) was performed on dried samples: (i) FLPs from CSE₃-F1 of $4.1 \pm 0.7 \mu\text{m}$ (Figure 2a) and (ii) bulk CSE₃-F1 polymer dried from its DCM-solution. The radially averaged SAXS data of both samples showed pronounced differences (Figure 4a). The FLPs exhibited scattering intensities at low scattering regimes of $q < 0.07 \text{ \AA}^{-1}$ (scaled with q^{-4} based on Porod's law), which are expected for huge dimensions and a large surface–volume ratio due to the presence of surface petals. For $q > 0.07 \text{ \AA}^{-1}$ the contribution from larger, microsized structures decreases and the scattering is dominated by the internal structure of the petals. No reliable signal was obtained for the bulk CSE₃-F1 polymer at $q < 0.02 \text{ \AA}^{-1}$ and thus the data points of $q < 0.02 \text{ \AA}^{-1}$ are missing.

Both samples showed a distinctive peak in the wide angle range at $q = 1.5 \text{ \AA}^{-1}$, corresponding to a correlation distance of $d = 4.1 \text{ \AA}$ (based on the approximation $d = 2\pi/q$). This value is in agreement with the average lateral distance between ordered hydrocarbon chains.^{26–28} Moreover, this Bragg peak is more pronounced for FLPs than for CSE₃-F1 polymer, indicating that more stearyl groups were involved in crystalline nanodomains within FLPs. A further peak at $q = 0.66 \text{ \AA}^{-1}$ corresponding to a real dimension of $\sim 9.6 \text{ \AA}$ is visible for FLPs, but not for CSE₃-F1 polymer. Nevertheless, a signal with a $q = 0.84 \text{ \AA}^{-1}$ corresponding to a distance of about 7 \AA is visible for CSE₃-F1 polymer. Probably, a less crystalline but a randomly coiled structure was formed during the drying process of CSE₃-F1 polymer.

The intermediate q range of $0.07\text{--}0.3 \text{ \AA}^{-1}$ is dominated by a few diffraction peaks, marked by stars in Figure 4a. These peaks are more pronounced for FLPs than for bulk CSE₃-F1 polymer. Their intensity ratio is approximately 1:2:3:..., which is in agreement with a lamellar crystal lattice.²⁹ The interlamellar distance was calculated to be $d = 68 \text{ \AA}$ for the FLPs. In contrast, the Bragg peaks in the intermediate scattering regime of CSE₃-F1 polymer are too smeared to clearly describe the lattice type. A spacing of $d = 54 \text{ \AA}$ was estimated for CSE₃-F1 polymer assuming the presence of similar lamellar crystal lattices. The scattering patterns of both samples exhibit minima at the same q values of 0.31 and 0.58 \AA^{-1} . This feature strongly suggests that these oscillations stem from the contribution of the same form factor due to the same (chemical) structure within FLPs and CSE₃-F1 polymer. The q values of 0.31 and 0.58 \AA^{-1} correspond to a real distance of $\sim 22 \text{ \AA}$, which is consistent with the length of stretched stearyl chains.³⁰ Thus, the lamellar structure is formed by stearyl groups via hydrophobic–hydrophobic interactions. The lamellae represent the building

Scheme 1. Schematic Illustration for the Formation of Flower-Like Particles (FLPs)^a

^aThe sizes are not in the real scale. See the text for more details.

blocks within FLPs and very probably also in dried CSE₃-F1 polymer, but to a less extent.

Model calculations were performed in order to further address the SAXS results (Figure 4b).²⁹ First, the scattering intensity of noninteracting platelets with a diameter of 100 Å (approximately the average contour length of the CSE₃-F1 chains with a DP_n of 18) and a thickness of 22 Å (the length of stretched stearyl groups) was involved. This model only describes the oscillations ascribed to the shape of nanostructures, which is known as form factor scattering. In the next step, interplatelet interactions were included using a lamellar spacing of the platelets. The separation distance was set at 66 Å, with a standard deviation of 10%. To describe the size of the nanopetals, five stacked platelets were further considered in the model. To reflect the low q range in the scattering of FLPs, where the scattering intensity follows the Porod's law ($\sim q^{-4}$), the scattering attributed to the contribution of porous surface petals of FLPs was included. As shown in Figure 4b, the final model well describes the features within the SAXS curve of CSE₃ FLPs.

The crystalline structure was further elucidated with long (100 ns) molecular dynamics simulations of the self-assembly of multiple CSE₃ chains in EA (4.8 wt %). Starting from completely different initial configurations, all simulations led to spontaneous precipitation and crystallization of stearyl side chains (Figures 4c,d, S14, and S15). The stearyl groups are ordered and form an approximately hexagonal packing. Interdigitation of stearyl groups belonging to different CSE₃ chains is observed in the crystalline clusters. The parallel stearyl groups within the ordered regions show an average distance of 4.4 ± 0.4 Å and an average length (alkyl groups only) of 19.6 ± 0.8 Å (Figure S16), which are in great agreement with the results from SAXS measurements (4.2 and 22 Å, respectively). In addition, the simulation showed that not all stearyl groups are involved in crystalline domains, which is also supported by the SAXS analysis.

Based on our experimental findings, a mechanism for the genesis of FLPs is proposed as in Scheme 1. The process starts with the evaporation of DCM ($T_b = 312.8$ K) from its mixture with EA ($T_b = 350.3$ K) and CSE₃. The solvent turns steadily

from a good to a poor solvent for CSE₃. During this process, CSE₃ chains interact with each other and precipitate out, while their stearyl side chains interdigitate and form ordered regions. Nascent clusters are formed by the aggregation of precipitated CSE₃ chains. Following the principles for the fractionation, CSE₃ chains of higher molecular weights precipitate out first, followed by CSE₃ chains of decreasing molecular weights.³¹ After the formation of initial templates, the CSE₃ chains grow on the particle surface and form nanopetals. Thereby, the precipitation of each CSE₃ fraction leaves a newly equilibrated solution. This process repeats until all DCM evaporate from the mixture. The three-dimensional nature of the space in the solvent mixture allows the nanopetals to grow in all possible directions. The formation of FLPs with branched nanostructures via crystallization is presumably governed by a kinetic rather than a thermodynamic process.^{32–34} Mass-transport and random nucleation are the steps limiting the crystal formation.^{35,36} Due to the gradual evaporation of DCM during the formation of FLPs, the CSE₃ chains have sufficient time to crystallize. The steps containing the precipitation of CSE₃ chains and the formation of ordered structures on the particle surface determine the formation of FLPs.³⁷ Too fast evaporation of DCM or too rash precipitation of CSE₃ chains, for example, by using strong precipitating agents such as ethanol and DMF, only led to irregular aggregates or nanoparticles (Figures S5–S8).

In summary, we demonstrated the successful preparation of novel, polymeric flower-like particles (FLPs) of 2.5–5 μm with hierarchical nanostructures on surface. The FLPs were formed using cellulose stearyl esters (CSEs) with degrees of substitution (DSs) of approximately 3, preferentially CSE with a DS of 3 (CSE₃) due to its defined chemical structure. FLPs show self-assembled ordered petal-like nanostructures at the particle surface. The formation of FLPs is strongly affected by the following key parameters: (i) DS of CSE which should be approximately 3, (ii) the molecular weight of CSE₃, (iii) the concentration of the CSE₃ solution, and (iv) the ratio of the good solvent dichloromethane to the precipitant, for example, ethyl acetate. The ordering of CSE₃ chains during the precipitation of CSE₃ chains from its solution is proposed to

be the mechanism behind the formation of FLPs. The ordered regions are formed by the crystallization of stearyl side chains, which form lamellar crystalline structures. After the initial formation of CSE₃ nuclei, other CSE₃ chains grow onto the surface leading to the formation of surface petals. Thus, we also provide a novel, facile technique for the preparation of hierarchical nanostructure through the crystallization of polymer side chains. Using this method, a new class of porous FLPs can be anticipated from readily available polymers showing versatile chemical structures and properties.

■ ASSOCIATED CONTENT

📄 Supporting Information

Detailed synthesis and analysis of cellulose stearyl esters as well as fabrication and more characterization of flower-like particles. This material is available free of charge via the Internet at <http://pubs.acs.org>.

■ AUTHOR INFORMATION

Corresponding Author

*Tel.: +49 6151 1675831. Fax: +49 6151 162479. E-mail: zhang@cellulose.tu-darmstadt.de.

Notes

The authors declare no competing financial interest.

■ ACKNOWLEDGMENTS

Authors thank the Hessian excellence initiative LOEWE – research cluster SOFT CONTROL (Hessen, Germany) for the financial support. We thank Prof. J.J. Schneider for the access to Zetasizer Nano ZS. We thank Prof. M. Biesalski for the kind support. Dr. M. Gallei and Ms. M. Trautmann are gratefully acknowledged for the DSC and SEC measurements.

■ REFERENCES

- (1) Ikkala, O.; ten Brinke, G. *Science* **2002**, *295*, 2407.
- (2) Kharisov, B. I. *Recent Pat. Nanotechnol.* **2008**, *2*, 190.
- (3) Noorduyn, W. L.; Grinthal, A.; Mahadevan, L.; Aizenberg, J. *Science* **2013**, *340*, 832.
- (4) Whitesides, G. M.; Grzybowski, B. *Science* **2002**, *295*, 2418.
- (5) Bao, Z.; Weatherspoon, M. R.; Shian, S.; Cai, Y.; Graham, P. D.; Allan, S. M.; Ahmad, G.; Dickerson, M. B.; Church, B. C.; Kang, Z.; Abernathy, H. W., 3rd; Summers, C. J.; Liu, M.; Sandhage, K. H. *Nature* **2007**, *446*, 172.
- (6) Lim, B.; Jiang, M.; Camargo, P. H.; Cho, E. C.; Tao, J.; Lu, X.; Zhu, Y.; Xia, Y. *Science* **2009**, *324*, 1302.
- (7) Peer, D.; Karp, J. M.; Hong, S.; FarokHzad, O. C.; Margalit, R.; Langer, R. *Nat. Nanotechnol.* **2007**, *2*, 751.
- (8) Wang, Z. L.; Song, J. *Science* **2006**, *312*, 242.
- (9) Cui, Y.; Wei, Q.; Park, H.; Lieber, C. M. *Science* **2001**, *293*, 1289.
- (10) Wang, Z.; Zhou, L.; David Lou, X. W. *Adv. Mater.* **2012**, *24*, 1903.
- (11) Ge, J.; Lei, J.; Zare, R. N. *Nat. Nanotechnol.* **2012**, *7*, 428.
- (12) Kharissova, O. V.; Kharisov, B. I. *Ind. Eng. Chem. Res.* **2010**, *49*, 11142.
- (13) Shao, M.; Ning, F.; Zhao, J.; Wei, M.; Evans, D. G.; Duan, X. J. *Am. Chem. Soc.* **2012**, *134*, 1071.
- (14) Nakanishi, T.; Ariga, K.; Michinobu, T.; Yoshida, K.; Takahashi, H.; Teranishi, T.; Möhwald, H.; D, G. K. *Small* **2007**, *3*, 2019.
- (15) Zhang, X.; Takeuchi, M. *Angew. Chem., Int. Ed.* **2009**, *48*, 9646.
- (16) Sun, J.; Ge, J.; Liu, W.; Lan, M.; Zhang, H.; Wang, P.; Wang, Y.; Niu, Z. *Nanoscale* **2014**, *6*, 255.
- (17) Wang, L. B.; Wang, Y. C.; He, R.; Zhuang, A.; Wang, X.; Zeng, J.; Hou, J. G. *J. Am. Chem. Soc.* **2013**, *135*, 1272.
- (18) Wang, Y.; Liu, Z. M.; Han, B. X.; Li, J. C.; Gao, H. X.; Wang, J. Q.; Zhang, J. L. *J. Phys. Chem. B* **2005**, *109*, 2605.
- (19) Landfester, K. *Angew. Chem.* **2009**, *121*, 4556.
- (20) Wang, W.; Zhang, M. J.; Xie, R.; Ju, X. J.; Yang, C.; Mou, C. L.; Weitz, D. A.; Chu, L. Y. *Angew. Chem., Int. Ed.* **2013**, *52*, 8084.
- (21) Gröschel, A. H.; Walther, A.; Lobling, T. I.; Schacher, F. H.; Schmalz, H.; Müller, A. H. *Nature* **2013**, *503*, 247.
- (22) Nie, Z.; Li, W.; Seo, M.; Xu, S.; Kumacheva, E. *J. Am. Chem. Soc.* **2006**, *128*, 9408.
- (23) Zhou, C.; Han, J.; Guo, R. *Macromolecules* **2008**, *41*, 6473.
- (24) Zhao, H.; Guo, X.; He, S.; Zeng, X.; Zhou, X.; Zhang, C.; Hu, J.; Wu, X.; Xing, Z.; Chu, L.; He, Y.; Chen, Q. *Nat. Commun.* **2014**, *5*, 3108.
- (25) Klemm, D.; Heublein, B.; Fink, H. P.; Bohn, A. *Angew. Chem., Int. Ed.* **2005**, *44*, 3358.
- (26) El Aziz, Y.; Bassindale, A. R.; Taylor, P. G.; Stephenson, R. A.; Hursthouse, M. B.; Harrington, R. W.; Clegg, W. *Macromolecules* **2013**, *46*, 988.
- (27) Grabner, D.; Hoffmann, H.; Forster, S.; Rosenfeldt, S.; Linders, J.; Mayer, C.; Talmon, Y.; Schmidt, J. *Adv. Colloid Interface Sci.* **2014**, *208*, 252.
- (28) Heeley, E. L.; Hughes, D. J.; El Aziz, Y.; Taylor, P. G.; Bassindale, A. R. *Macromolecules* **2013**, *46*, 4944.
- (29) Förster, S.; Fischer, S.; Zielske, K.; Schellbach, C.; Sztucki, M.; Lindner, P.; Perlich, J. *Adv. Colloid Interface Sci.* **2011**, *163*, 53.
- (30) Kasai, W.; Kuga, S.; Magoshi, J.; Kondo, T. *Langmuir* **2005**, *21*, 2323.
- (31) Shultz, A. R.; Flory, P. J. *J. Am. Chem. Soc.* **1952**, *74*, 4760.
- (32) Lim, B.; Xiong, Y.; Xia, Y. *Angew. Chem., Int. Ed.* **2007**, *46*, 9279.
- (33) Witten, T.; Sander, L. *Phys. Rev. Lett.* **1981**, *47*, 1400.
- (34) Zeng, J.; Xia, Y. *Nat. Nanotechnol.* **2012**, *7*, 415.
- (35) Liu, X. Y.; Boek, E. S.; Briels, W. J.; Bennema, P. *Nature* **1995**, *374*, 342.
- (36) Zhang, T. H.; Liu, X. Y. *Angew. Chem., Int. Ed.* **2009**, *48*, 1308.
- (37) Erdemir, D.; Lee, A. Y.; Myerson, A. S. *Acc. Chem. Res.* **2009**, *42*, 621.